



UNIVERSIDADE ESTADUAL DE CAMPINAS
SISTEMA DE BIBLIOTECAS DA UNICAMP
REPOSITÓRIO DA PRODUÇÃO CIENTÍFICA E INTELLECTUAL DA UNICAMP

Versão do arquivo anexado / Version of attached file:

Versão do Editor / Published Version

Mais informações no site da editora / Further information on publisher's website:

<https://www.osapublishing.org/oe/abstract.cfm?uri=oe-25-14-16484>

DOI: 10.1364/OE.25.016484

Direitos autorais / Publisher's copyright statement:

©2017 by Optical Society of America. All rights reserved.

DIRETORIA DE TRATAMENTO DA INFORMAÇÃO

Cidade Universitária Zeferino Vaz Barão Geraldo

CEP 13083-970 – Campinas SP

Fone: (19) 3521-6493

<http://www.repositorio.unicamp.br>



Hybrid multimode resonators based on grating-assisted counter-directional couplers

JORDAN A. DAVIS,^{1,*} ANDREW GRIECO,¹ MARIO C. M. M. SOUZA,^{1,2}
NEWTON C. FRATESCHI,² AND YESHAIAHU FAINMAN¹

¹Department of Electrical & Computer Engineering, University of California, San Diego, 9500 Gilman Dr., La Jolla, California 92023, USA

²Instituto de Física Gleb Wataghin, Universidade Estadual de Campinas, 13083-970 Campinas, São Paulo, Brazil

*jad022@ucsd.edu

Abstract: Research thrusts in silicon photonics are developing control operations using higher order waveguide modes for next generation high-bandwidth communication systems. In this context, devices allowing optical processing of multiple waveguide modes can reduce architecture complexity and enable flexible on-chip networks. We propose and demonstrate a hybrid resonator dually resonant at the 1st and 2nd order modes of a silicon waveguide. We observe 8 dB extinction ratio and modal conversion range of 20 nm for the 1st order quasi-TE mode input.

© 2017 Optical Society of America

OCIS codes: (130.3120) Integrated optics devices; (050.0050) Diffraction and gratings; (130.7408) Wavelength filtering devices.

References and links

1. S. Chakravarty, A. Hosseini, X. Xu, L. Zhu, Y. Zou, and R. T. Chen, "Analysis of ultra-high sensitivity configuration in chip-integrated photonic crystal microcavity bio-sensors," *Appl. Phys. Lett.* **104**(19), 191109 (2014).
2. P. Dong, J. Lee, Y. Chen, L. L. Buhl, S. Chandrasekhar, J. H. Sinsky, and K. Kim, "Four-Channel 100-Gb/s per Channel Discrete Multi-Tone Modulation Using Silicon Photonic Integrated Circuits," in *OFC 2015* (2015), paper Th5B.4.
3. M. Veldhorst, J. C. C. Hwang, C. H. Yang, A. W. Leenstra, B. de Ronde, J. P. Dehollain, J. T. Muhonen, F. E. Hudson, K. M. Itoh, A. Morello, and A. S. Dzurak, "An addressable quantum dot qubit with fault-tolerant control-fidelity," *Nat. Nanotechnol.* **9**(12), 981–985 (2014).
4. A. Griffith, J. Cardenas, C. B. Poitras, and M. Lipson, "High quality factor and high confinement silicon resonators using etchless process," *Opt. Express* **20**(19), 21341–21345 (2012).
5. M. Ye, Y. Yu, G. Chen, Y. Luo, and X. Zhang, "On-chip WDM mode-division multiplexing interconnection with optional demodulation function," *Opt. Express* **23**(25), 32130–32138 (2015).
6. G. F. R. Chen, T. Wang, K. J. A. Ooi, A. K. L. Chee, L. K. Ang, and D. T. H. Tan, "Wavelength selective mode division multiplexing on a silicon chip," *Opt. Express* **23**(6), 8095–8103 (2015).
7. A. Mohanty, M. Zhang, A. Dutt, S. Ramelow, P. Nussenzveig, and M. Lipson, "Quantum Interference between Transverse Spatial Waveguide Modes," in *CLEO 2015* (2015), paper FTu4A.5.
8. B. Stern, X. Zhu, C. P. Chen, L. D. Tzuang, J. Cardenas, K. Bergman, and M. Lipson, "On-chip mode-division multiplexing switch," *Optica* **2**(6), 530 (2015).
9. C. Williams, B. Banan, G. Cowan, and O. Liboiron-Ladouceur, "A Source-Synchronous Architecture Using Mode-Division Multiplexing for On-Chip Silicon Photonic Interconnects," *IEEE J. Sel. Top. Quantum Electron.* **22**(6), 8300109 (2016).
10. Y. Ho, D. Lee, J. Cardenas, and M. Lipson, "Linear silicon PN junction phase modulator," in *CLEO 2015* (2015), paper SW3N.5.
11. C. H. Cox, E. I. Ackerman, G. E. Betts, and J. L. Prince, "Limits on the performance of RF-over-fiber links and their impact on device design," *IEEE Trans. Microw. Theory Tech.* **54**(2), 906–920 (2006).
12. G. Chen, Y. Yu, and X. Zhang, "Monolithically mode division multiplexing photonic integrated circuit for large-capacity optical interconnection," *Opt. Lett.* **41**(15), 3543–3546 (2016).
13. T. Mulugeta and M. Rasras, "Silicon hybrid (de)multiplexer enabling simultaneous mode and wavelength-division multiplexing," *Opt. Express* **23**(2), 943–949 (2015).
14. L.-W. Luo, N. Ophir, C. P. Chen, L. H. Gabrielli, C. B. Poitras, K. Bergman, and M. Lipson, "WDM-compatible mode-division multiplexing on a silicon chip," *Nat. Commun.* **5**, 3069 (2014).
15. B. A. Dorin and W. N. Ye, "Two-mode division multiplexing in a silicon-on-insulator ring resonator," *Opt. Express* **22**(4), 4547–4558 (2014).

16. J. D. Love and N. Riesen, "Single-, Few-, and Multimode Y-Junctions," *J. Lightwave Technol.* **30**(3), 304–309 (2012).
17. A. Y. Piggott, J. Lu, K. G. Lagoudakis, J. Petykiewicz, T. M. Babinec, and J. Vučković, "Inverse design and demonstration of a compact and broadband on-chip wavelength demultiplexer," *Nat. Photonics* **9**(6), 374–377 (2015).
18. L. F. Frellsen, Y. Ding, O. Sigmund, and L. H. Frandsen, "Topology optimized mode multiplexing in silicon-on-insulator photonic wire waveguides," *Opt. Express* **24**(15), 16866–16873 (2016).
19. A. Grieco, G. Porter, and Y. Fainman, "Integrated space-division multiplexer for application to data center networks," *IEEE J. Sel. Top. Quantum Electron.* **22**(6), 2361 (2016).
20. H. Qiu, J. Jiang, P. Yu, T. Dai, J. Yang, H. Yu, and X. Jiang, "Silicon band-rejection and band-pass filter based on asymmetric Bragg sidewall gratings in a multimode waveguide," *Opt. Lett.* **41**(11), 2450–2453 (2016).
21. W. Shi, X. Wang, C. Lin, H. Yun, Y. Liu, T. Baehr-Jones, M. Hochberg, N. A. F. Jaeger, and L. Chrostowski, "Silicon photonic grating-assisted, contra-directional couplers," *Opt. Express* **21**(3), 3633–3650 (2013).
22. J. St-Yves, H. Bahrami, P. Jean, S. LaRochelle, and W. Shi, "Widely bandwidth-tunable silicon filter with an unlimited free-spectral range," *Opt. Lett.* **40**(23), 5471–5474 (2015).
23. J.-P. Weber, "Spectral characteristics of coupled-waveguide Bragg-reflection tunable optical filter," *IEE Proc., J. Optoelectron.* **140**(5), 275–284 (1993).
24. W. Shi, V. Veerasubramanian, D. V. Plant, N. A. F. Jaeger, and L. Chrostowski, "Silicon photonic Bragg-grating couplers for optical communications," *Optoelectron. Devices Mater.* **9**10, 90100F (2014).
25. K. Ikeda, M. Nezhad, and Y. Fainman, "Wavelength selective coupler with vertical gratings on silicon chip," *Appl. Phys. Lett.* **92**(20), 20–23 (2008).
26. R. Boeck, M. Caverley, L. Chrostowski, and N. A. F. Jaeger, "Process calibration method for designing silicon-on-insulator contra-directional grating couplers," *Opt. Express* **23**(8), 10573–10588 (2015).
27. M. T. Boroojerdi, M. Ménard, and A. G. Kirk, "Two-period contra-directional grating assisted coupler," *Opt. Express* **24**(20), 22865–22874 (2016).
28. C. A. Barrios, V. R. Almeida, R. R. Panepucci, B. S. Schmidt, and M. Lipson, "Compact Silicon Tunable Fabry – Pérot Resonator With Low Power Consumption," *IEEE Photonics Technol. Lett.* **16**(2), 506–508 (2004).
29. A. Grieco and Y. Fainman, "Characterization of distributed Bragg reflectors," *J. Quantum Elect.* **50**(6), 453–457 (2014).
30. X. Chen, M. Mohamed, Z. Li, L. Shang, and A. R. Mickelson, "Process variation in silicon photonic devices," *Appl. Opt.* **52**(31), 7638–7647 (2013).
31. L. Chrostowski and M. Hochberg, *Silicon Photonics Design* (2015).
32. R. Boeck, M. Caverley, L. Chrostowski, and N. A. F. Jaeger, "Process calibration method for designing silicon-on-insulator contra-directional grating couplers," *Opt. Express* **23**(8), 10573–10588 (2015).

1. Introduction

Integrated photonics has dramatically evolved in the past decades and is now a major enabling technology for applications ranging from sensing to optical interconnects and integrated quantum computing [1–3]. Traditional photonic circuitry has been developed using single mode waveguides that allow very compact devices and low optical losses [4]. More recently, there have been increasing efforts to develop architectures compatible with multimode waveguide operation [5–7]. One major motivation is the implementation of integrated mode-division multiplexing (MDM), which promises large bandwidth scaling for on-chip communication systems [8,9]. In addition to MDM, the linearity of depletion-based silicon modulators can be significantly enhanced when high order modes are employed [10] which represents an important advancement for on-chip analog photonic links [11].

Proposed multimode architectures have been mostly based on single mode components combined with mode converters [8,12]. This approach benefits from the advancements in single mode devices, but at the cost of complexity and footprint size. For instance, mode/wavelength (de)multiplexers can be passively realized using phase matched directional couplers [13], ring resonators [8,14,15], Y-junctions [16], inverse design [17,18], or grating-assisted counter-directional couplers (GACDC) [6,15,19,20], but active signal processing such as electro-optic modulation is still mainly performed using single mode components such as resonators [8,12]. After the signal has been processed, mode conversion is performed once again. As the number of spatial and spectral channels scales up so does the required number of components, but at a much faster rate. In this scenario, components that facilitate active optical processing of different transversal modes could have an important impact in reducing complexity and increasing flexibility for future MDM networks on a chip.

In this paper we demonstrate a hybrid resonator that supports longitudinal modes composed by different transversal mode orders. The device is based on GACDC resonators [21] and offers both precision in design and wavelength selectivity while retaining the footprint advantage of GACDC, allowing for compact architectures. The fabricated device is resonant at the 1st (TE_0) and 2nd (TE_1) guided modes.

2. Grating-Assisted Counter-Directional Resonators

GACDC operate as four-port Bragg reflectors that produce a spectral stop band in the through-port, a transmission window at the drop-port, and negligible add-port transmission when the phase-matching condition is met [22]. They consist of closely spaced waveguides with periodic sidewall perturbations (grating) that act as counter-directional mirrors on either side of a cavity created by an unperturbed waveguide section, as depicted in Fig. 1(a). In this example, the waveguide widths w_1 and w_2 are chosen to allow single mode operation in waveguide 1 and multimode operation in waveguide 2, while the grating is designed to allow phase-matching between the forward-propagating fundamental mode (TE_0) of waveguide 1 and the backward-propagating second order mode (TE_1) of waveguide 2 around a targeted wavelength λ_0 . At phase-matching, the grating period Λ is related to λ_0 and to the effective indices n_1 and n_2 of the two modes by the well-known relation [23–27]

$$\Lambda(n_1 + n_2) = \lambda_0 \quad (1)$$

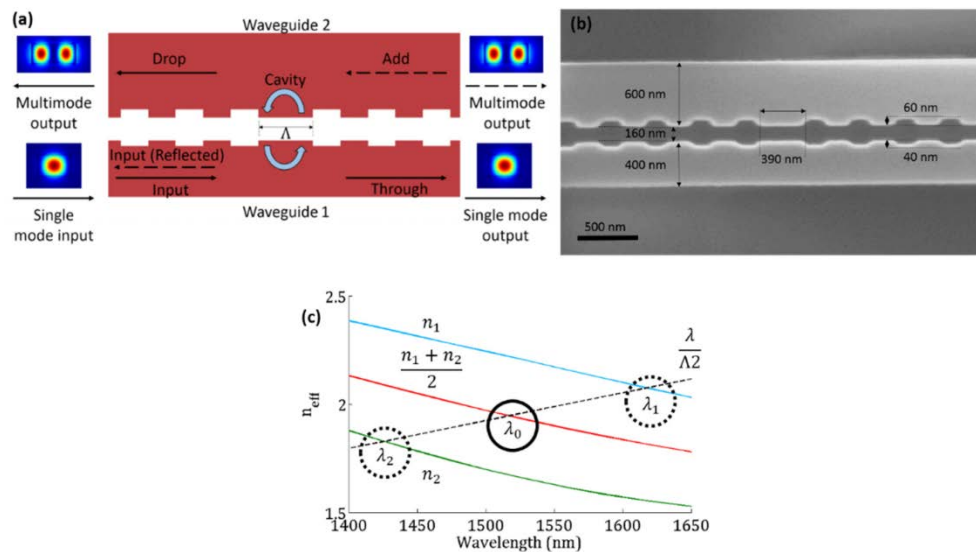


Fig. 1. (a) Schematics of a hybrid multimode resonator. Periodic perturbations with a 50% duty cycle create mirrors that routes light to the through-port (on resonance) or the drop-port (off resonance). On resonance injected light from the input circulates in the cavity between the single mode and multimode waveguides. The cavity length is equal to one period length, Λ , of the mirror. Curved arrows in the cavity correspond to the resonant directionality of light. (b) Scanning electron microscope image of the cavity and surrounding mirrors. (c) Dispersion curves for a waveguide of 400 nm (n_1), 600 nm (n_2), and the average of the two indices. The phase matching condition is shown by the intersection with the dashed black line.

In addition, phase-matching between forward- and backward-propagating modes of waveguides 1 and 2 can also occur at $\lambda_1 = 2\Lambda n_1$ and $\lambda_2 = 2\Lambda n_2$, respectively. These multiple phase-matching conditions are graphically represented in Fig. 1(c) as the intersection of the dispersive effective indices $n_1(\lambda)$, $n_2(\lambda)$ and their average (solid lines) with the wavelength normalized by the grating period $\lambda/(2\Lambda)$ (dashed line) for waveguide widths $w_1 = 400$ nm and $w_2 = 600$ nm and grating period $\Lambda = 390$ nm.

GACDC present great design flexibility that make them strong candidates for hitless, densely packed MDM/WDM switching. As shown in Fig. 1(c), the grating coupler can be designed so that only λ_0 falls within the telecommunication band, mitigating deleterious effects of back-reflections into other wavelength channels. In addition, the high propagation constant mismatch between the waveguides prevents energy transfer by directional coupling allowing dense photonic circuitry with low crosstalk. Finally, the GACDC design has potential to be scaled up to multiple waveguides as well as different waveguide mode orders by designing waveguides with larger widths and locally altering the mirror period. Increasing the width w_2 introduces phase matched conditions to excite additional higher spatial modes, as previously demonstrated in a non-resonant structure [6]. The introduction of a defect or an unperturbed waveguide section between identical GACDC create a resonant cavity (Fig. 1(a)). Differently from a typical standing-wave Fabry-Pérot cavity formed by a defect on a single waveguide [28], however, this “hybrid resonator” is a travelling-wave resonator formed by two distinct transversal modes, in this case TE_0 and TE_1 , which propagate in opposite direction in different waveguides and couple in the grating sections.

The width of the waveguides is chosen to allow a single mode through-port and a multimodal drop-port structures, respectively. Sidewall perturbations are chosen to be 10% of the waveguide width to limit reflection of the input before entering the cavity. A device length of 60 periods per mirror is chosen to provide a near critical coupling condition of the resonance for both the through and drop-ports. The total device footprint is $54.5 \mu\text{m}^2$.

The device is simulated using the finite difference time domain (FDTD) tool Lumerical FDTD to estimate interactions between the input source and the perturbations of the counter-directional coupler. Figure 2(a) shows the simulated spectra of the device assuming a lossless waveguide. The extinction ratio of the through-port is over 20 dB while the drop-port has an extinction ratio of 10 dB. There is a loss of 1 dB as measured from the drop-port when the waveguides are phase matched due to the back reflections caused by the gratings of the single mode waveguide into the input. The add-port is designed to be below 15 dB of the maximum power since light in the multimode waveguide is propagating in the opposite direction towards the drop-port. The power seen from the add-port is due to the backward reflections of the light interacting with the mirror in the multimode waveguide. On resonance the power density of light increases in the cavity, seen in Fig. 2(b), where two spatial modes are excited.

The devices are fabricated using a silicon-on-insulator substrate with a 220 nm thick silicon device layer on 3 μm of buried oxide. Waveguides are patterned using electron beam lithography and etched using reactive ion plasma etching. The devices are cladded with silicon dioxide using plasma-enhanced chemical vapor deposition.

The spectrum of the device is measured by edge coupling a tapered single mode fiber to the input and collecting the output light with an objective lens, which is routed to a power detector. The light emitted from the fiber is quasi-TE polarized. To image the optical modes the power detector is replaced with a camera sensitive to near IR light. Each output is normalized to the output of the single mode.

3. Measured Resonator Responses

Measured spectra, seen in Fig. 2(b), match the simulated spectra shown in Fig. 2(a). The single mode output displays a relatively flat passband and a peak extinction ratio of 11 dB. The multimode resonance has a peak extinction ratio of 8 dB, which agrees with the simulated results. The stopband and resonance is created by the phase matching between the 1st and 2nd modes in the through and drop-ports. Differences between the simulated and measured spectra, such as lower extinction ratio seen in the through-port and intensity of the drop-port, can be attributed to loss incurred by the multimodal waveguide. The 2nd mode, which is less confined in the waveguide than the 1st mode, has higher interaction with the waveguide sidewalls and scatters light. Scattering loss can be reduced by oxidizing the waveguides after etching. Additional loss is due to mode mismatch between the Bloch modes of the periodically perturbed

Bragg reflectors and the modes of the unperturbed waveguide that forms the resonant cavity. It can be alleviated by adiabatically tapering the transition between the two structures [29]. At the resonant wavelength of the cavity, the optical field alternates between the two waveguides, forming a guided resonance in the counter clockwise direction. As expected the add-port presents only a residual amount of power compared to the through-port due to the phase matching between the two waveguides. The full width at half maximum is 1.4 nm, providing a loaded quality factor of ~ 1100 . The stopband provides modal conversion over a bandwidth of 20 nm, seen in Fig. 2(b).

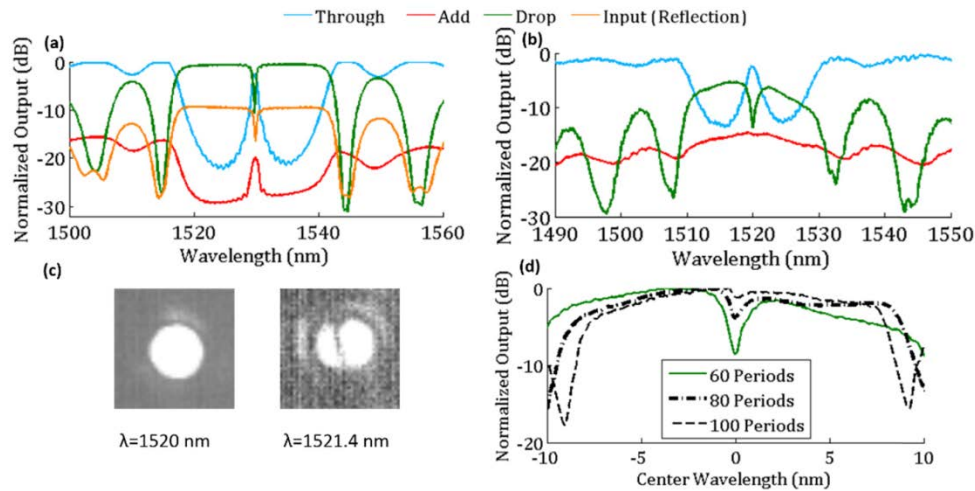


Fig. 2. (a) Simulated and (b) measured spectral response for the 1st order quasi-TE over the phase matched region for the through, drop, and add-ports. (c) Associated images of the 1st and 2nd order modes at the output of the through-port (on resonance) and drop-port (off resonance), respectively. (d) Measured drop-port spectra of multiple resonators with varying mirror period length.

There exists a critically coupled regime of the resonator where the round-trip loss within the cavity is balanced by the light coupled into and out of the cavity. To investigate the effects of the coupling on the extinction ratio the resonances the mirror length is altered. Figure 2(d) shows the experimental effect of increasing the mirror length for a resonator of set period length and waveguide width. The spectra are normalized to a center wavelength to adjust for fabrication differences across multiple devices. From the fabricated devices, 60 periods (23.6 μm) per mirror allows an extinction ratio of 8 dB, suggesting the device is close to critical coupling for the multimode port. As the mirror length is increased the extinction ratio decreases due to increased coupling of the input directly to the multimode output without interacting with the cavity, vastly under coupling the light. Slightly decreasing the mirror length to 50 periods per mirror can potentially critically couple the resonator, while a further reduction could undesirably over couple the resonator.

The cavity can be extended to arbitrary lengths, allowing the free spectral range (FSR) to be controlled. We define the FSR of the resonator to be

$$FSR = \frac{\lambda^2}{n_g L} \quad (2)$$

where L is the round-trip length of the cavity. As the length of the cavity increases the FSR decreases as seen in Fig. 3 where the cavity has been extended to 200 μm . As a result, multiple resonances are detectable in the stopband of the device. The round-trip loss increases, which reduces the extinction ratio of the resonances as measured from the drop-port. The through-port continues to support large extinction ratios due to the lower loss seen in the lower order mode.

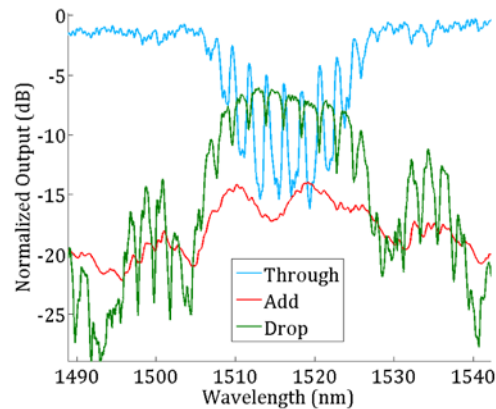


Fig. 3. Measured spectra of a resonator with a 200- μm -long cavity and mirrors with 60 periods.

4. Discussion

This device has potential application in multiplexing by concatenating multiple resonators operating at different wavelengths, as seen in Fig. 4. Input signals at the resonant wavelength of a device are converted to higher order spatial modes and routed to the drop port. Drop port signals can be forwarded to the add port of the following device, designed to be resonant at a different wavelength, combining multiple signals into a single waveguide. This approach can be scaled by including additional spatial modes. Mode conversion to the 5th order mode has been demonstrated in directional couplers [6], suggesting more than two modes can be used simultaneously, by increasing the waveguide width and altering the grating period of the mirrors.

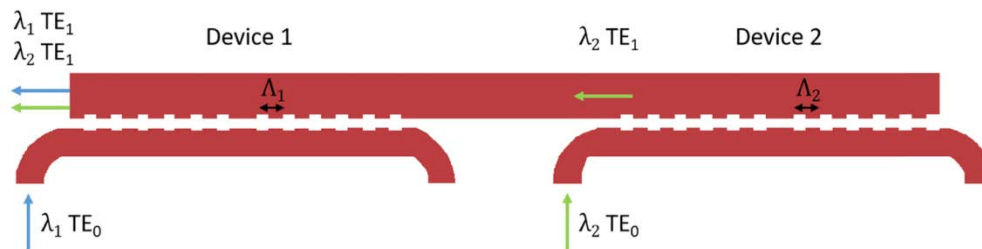


Fig. 4. Two concatenated devices that are resonant at different wavelengths as determined by the grating periods. Slightly detuning each device from resonance allows the TE_1 mode from device 2 to be injected into the add port of device 1, allowing co-propagation of two TE_1 modes at different wavelengths in a single waveguide.

Silicon photonics is a high-index-contrast platform and, as a result, the devices are quite sensitive to fabrication variations [30] and imperfections. For the hybrid resonators, the tolerance is mainly dictated by the grating sections. These fine structures are hardly reproduced with fidelity by the lithography tools and the resulting experimental device often deviates from the design. Methods based on computational lithography [31] and empirical models [31,32] can be employed in the design process to overcome strong discrepancies. This is especially important for achieving high extinction ratio and a desired bandwidth as they are dictated by the coupling strength which in turn depends on the sidewall modulation and on the grating length (or the number of periods). On the other hand, variations on the overall waveguide width and on the grating period will affect the central wavelength of the stop band, which can be compensated by the use of index tuning structures such as integrated microheaters.

As mentioned previously, the hybrid resonator could be an interesting candidate for optical modulation in MDM systems. For such application, extinction ratios higher than the

demonstrated 8 dB are desired. Internal losses and strong intra-waveguide reflections are predominately responsible for non-ideal extinction ratios and affect our device. Previous work [21] has shown losses of 5 dB/cm can drastically reduce the extinction ratio compared to a lossless device. As shown in Fig. 5, the extinction ratio can be increased by optimizing the fabrication process for loss reduction. Devices with small FSRs, which suffer from high loss in the long cavity required to create small FSR, would also benefit from a reduction of loss. In these devices the incurred loss is higher which provides a lower extinction ratio.

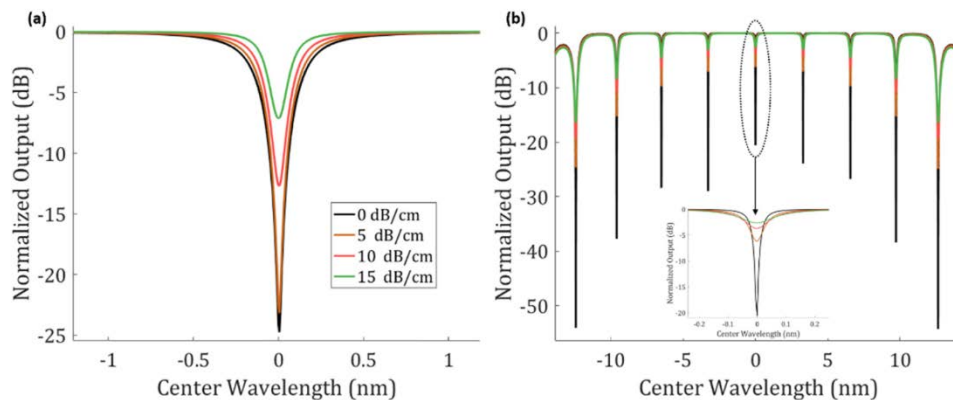


Fig. 5. Simulated spectral response of the resonances as seen from the drop-port for a device with (a) cavity length of $\Lambda/2$ and (b) cavity length of $100 \mu\text{m}$. (Inset) Enlarged image of the central resonance for a device with cavity length $100 \mu\text{m}$. Device performance, as determined by the extinction ratio, can be potentially improved by reducing internal losses.

In conclusion, we have simulated and experimentally demonstrated a four-port resonator that couples between the 1st and 2nd order quasi-TE modes. Our device is compact and can be integrated into dense design architectures. The device is designed to have a resonant wavelength within the near IR range and can be tailored to be resonant over a vast range of wavelengths by changing the grating period. Additionally, the design can be extended to include additional modes, increasing the effectiveness of MDM. Furthermore, the cavity can be chosen with arbitrary length allowing free design of the free spectral range. Due to the flexibility in design, such hybrid multimode resonators based on grating-assisted counter-directional couplers are a promising alternative to traditional resonators.

Funding

Office of Naval Research (ONR) Multi-Disciplinary Research Initiative; National Science Foundation (NSF) (NNCI-SDNI, ERC CIAN); Defense Advanced Research Projects Agency (DARPA); Army Research Office (ARO); Cymer Corporation. M. Souza acknowledges FAPESP (grant 2015/20525-6).

Acknowledgments

This work was performed in part at the San Diego Nanotechnology Infrastructure (SDNI) of UCSD, a member of the National Nanotechnology Coordinated Infrastructure, which is supported by the National Science Foundation (Grant ECCS-1542148). We thank M. Montero for technical assistance regarding the fabrication.